The Astrophysical Journal Letters, 884:L33 (5pp), 2019 October 20 https://doi.org/10.3847/2041-8213/ab4815

The ALMaQUEST Survey: The Molecular Gas Main Sequence and the Origin of the Star-forming Main Sequence

Lihwai Lin[1], Hsi-An Pan[1], Sara L. Ellison[2], Francesco Belfiore[3], Yong Shi[4,5], Sebastián F. Sánchez[6], Bau-Ching Hsieh[1], Kate Rowlands[7], S. Ramya[8], Mallory D. Thorp[2], Cheng Li[9], and Roberto Maiolino[10,11]
[1] Institute of Astronomy & Astrophysics, Academia Sinica, Taipei 10617, Taiwan; lihwailin@asiaa.sinica.edu.tw
[2] Department of Physics & Astronomy, University of Victoria, Finnerty Road, Victoria, BC V8P 1A1, Canada
[3] European Southern Observatory, Karl-Schwarzschild-Str. 2, Garching bei München, D-85748, Germany
[4] School of Astronomy and Space Science, Nanjing University, Nanjing 210093, People's Republic of China
[5] Key Laboratory of Modern Astronomy and Astrophysics (Nanjing University), Ministry of Education, Nanjing 210093, People's Republic of China
[6] Instituto de Astronomía, Universidad Nacional Autónoma de México, Circuito Exterior, Ciudad Universitaria, Ciudad de México 04510, Mexico
[7] Department of Physics & Astronomy, Johns Hopkins University, Bloomberg center, 3400 N. Charles Street, Baltimore, MD 21218, USA
[8] Indian Institute of Astrophysics, II Block, Koramangala, Bengaluru 560 034, India
[9] Tsinghua Center for Astrophysics and Physics Department, Tsinghua University, Beijing 100084, People's Republic of China
[10] Cavendish Laboratory, University of Cambridge, 19 J. J. Thomson Avenue, Cambridge CB3 0HE, UK
[11] University of Cambridge, Kavli Institute for Cosmology, Cambridge, CB3 0HE, UK
Received 2019 August 7; revised 2019 September 23; accepted 2019 September 24; published 2019 October 14

Abstract

The origin of the star-forming main sequence (SFMS; i.e., the relation between star formation rate and stellar mass, globally or on kpc scales) remains a hotly debated topic in galaxy evolution. Using the ALMA-MaNGA QUEnching and STar formation (ALMaQUEST) survey, we show that for star-forming spaxels in the main-sequence galaxies, the three local quantities, star formation rate surface density ($\Sigma_{\rm SFR}$), stellar mass surface density (Σ_*), and the H_2 mass surface density ($\Sigma_{\rm H_2}$) are strongly correlated with one another and form a 3D linear (in log) relation with dispersion. In addition to the two well-known scaling relations, the resolved SFMS ($\Sigma_{\rm SFR}$ versus Σ_*) and the Schmidt–Kennicutt (SK) relation ($\Sigma_{\rm SFR}$ versus $\Sigma_{\rm H_2}$), there is a third scaling relation between $\Sigma_{\rm H_2}$ and Σ_*, which we refer to as the molecular gas main sequence (MGMS). The latter indicates that either the local gas mass traces the gravitational potential set by the local stellar mass or both quantities follow the underlying total mass distributions. The scatter of the resolved SFMS ($\sigma \sim 0.25$ dex) is the largest compared to those of the SK and MGMS relations ($\sigma \sim 0.2$ dex). A Pearson correlation test also indicates that the SK and MGMS relations are more strongly correlated than the resolved SFMS. Our result suggests a scenario in which the resolved SFMS is the least physically fundamental and is the consequence of the combination of the SK and the MGMS relations.

Key words: galaxies: evolution – galaxies: general – galaxies: star formation

1. Introduction

The discovery of the tight relation between the star formation rate and the stellar mass of galaxies, namely, the star-forming main sequence (SFMS; Brinchmann et al. 2004; Daddi et al. 2007; Noeske et al. 2007; Lin et al. 2012; Whitaker et al. 2012; Speagle et al. 2014), not only offers a channel to characterize properties of galaxies but also provides constraints on the galaxy formation and evolution models. However, the physics driving this scaling relation are not well understood, as it is not clear why the current star formation rate is related to the total star formation rate integrated over the past (i.e., stellar mass). Star formation is a complex process that involves multiple scales. For example, whereas the global star formation rate depends on the large-scale environment (Dressler 1980; Kauffmann et al. 2004; Cooper et al. 2007; Elbaz et al. 2007; Lin et al. 2014), the efficiency of gas converted into stars is dependent on local conditions operating on sub-kpc scales (Krumholz & McKee 2005; Murray 2011). Probing relationships between stars and gas across different physical scales may therefore shed light on the origin of the SFMS.

Recent studies using integral field spectroscopy observations have shown that the star formation rate surface density ($\Sigma_{\rm SFR}$) traces the stellar mass surface density (Σ_*) linearly at kpc/sub-kpc scales (Sánchez et al. 2013; Wuyts et al. 2013; Cano-Díaz et al. 2016; Hsieh et al. 2017; Ellison et al. 2018; Medling et al. 2018; Pan et al. 2018; Vulcani et al. 2019). This so-called "resolved" SFMS (rSFMS) indicates that the connection between the global star formation rate and stellar mass may actually originate from local processes. However, while the relationship between $\Sigma_{\rm H_2}$ and $\Sigma_{\rm SFR}$ (Schmidt–Kennicutt, or SK, relation; Schmidt 1959; Kennicutt 1998) is understood as the formation of stars from molecular gas, the physical reason for the rSFMS remains a mystery. To complete the picture of the origin of rSFMS, it is therefore vital to relate the molecular gas to star formation tracers and stellar masses with the same spatial resolution. In this work, we combine spatially resolved observations from the Mapping Nearby Galaxies at Apache Point Observatory (MaNGA; Bundy et al. 2015) and Atacama Large Millimeter/submillimeter Array (ALMA) for 14 SFMS galaxies at $z \sim 0.03$, which allow us to study the relationships between the surface densities of star formation rate, molecular gas, and stellar mass on kpc scales.

Throughout this Letter we adopt the following cosmology: $H_0 = 70\ {\rm km\ s^{-1}\ Mpc^{-1}}$, $\Omega_m = 0.3$, and $\Omega_\Lambda = 0.7$. We use a Salpeter initial mass function (IMF).

2. Sample and Observations

The ALMA-MaNGA QUEnching and STar formation survey (ALMaQUEST; L. Lin et al. 2019, in preparation) is a compilation of four ALMA PI programs that follow up MaNGA galaxies with ^{12}CO(1 − 0) at a spatial resolution matched to MaNGA (FWHM $\sim 2\farcs5$). The "Quenching" component

(2015.1.01225.S, 2017.1.01093.S, and 2018.1.00558.S; PI:L. Lin) of ALMaQUEST targets 32 galaxies that are on the main sequence (MS; $\sim 1/3$ of the sample) and those in the green valley ($\sim 2/3$ of the sample). The other component, "Starburst" program (2018.1.00541.S; PI: S. Ellison), consists of 12 central starburst galaxies and 4 regular MS galaxies (see S. Ellison et al. 2019, in preparation). All of these observations adopt identical observing setups and reduction procedures. In this work, we present results using 14 MS galaxies with $10 < \log(M_*/M_\odot) < 11.5$ taken from the ALMaQUEST survey. These galaxies are selected to have $10^{-10.5}$ yr^{-1} < specific star formation rate (sSFR) < $10^{-9.5}$ yr^{-1} without showing strong central starburst features. The sSFR range is sufficiently broad to ensure that we sample a variety of star-forming galaxies. The CO data are processed following the procedures described in Lin et al. (2017), and the details will be described in the ALMaQUEST survey paper (L. Lin et al. 2019, in preparation). The H_2 mass surface density (Σ_{H_2}) is computed from the inclination-corrected CO surface density by adopting a conversion factor (α_{CO}) of 4.3 $M_\odot$ (K km s^{-1} pc^2)$^{-1}$ (e.g., Bolatto et al. 2013). A signal-to-noise ratio (S/N) > 2 cut[12] in the CO line is applied to our analysis.

Other measurements, such as Σ_* and emission-line fluxes, are obtained from the MaNGA Data Release 15 (DR15) data cubes processed by the Pipe3D pipeline (Sánchez et al. 2016). All the emission lines were then dust extinction corrected using the Balmer decrement computed at each spaxel, following the method described in the Appendix of Vogt et al. (2013). An extinction law with Rv = 4.5 (Fischera & Dopita 2005) is used. The SFR is estimated based on this extinction-corrected Hα flux using the conversion given by Kennicutt (1998) with the Salpeter IMF. Σ_* and Σ_{SFR} are computed using the stellar mass and SFR derived for each spaxel, normalized to the physical area of one spaxel with the inclination correction applied. We limit our sample to spaxels with $\Sigma_* > 10^7\ M_\odot$ kpc^{-2} and require the S/N in strong lines (Hα and Hβ) and in weak lines ([N II] 6584 and [O III] 5007) to be > 3 and > 2, respectively. These spaxels are further classified as star-forming regions using the [N II] 6584 diagnostic, following the method of Kauffmann et al. (2003).

3. Results

3.1. The 3D and 2D Scaling Relations between Σ_{SFR}, Σ_{H_2}, and Σ_*

We first made a 3D plot (Figure 1) to show the spaxel-to-spaxel relationship between Σ_{SFR}, Σ_*, and Σ_{H_2} for star-forming spaxels identified using the diagnostic described in Section 2. Figure 1 shows that these three quantities form a 3D linear (in log) relation with dispersion, suggesting that each pair of these three variables forms a tight relation. This is further illustrated by the three contours that represent the deprojected data points on the Σ_{SFR}–Σ_*(red), Σ_{SFR}–Σ_{H_2} (blue), and Σ_{H_2}–Σ_* (orange) planes. In addition to the well-known SK relation (Σ_{SFR} versus Σ_{H_2}) and resolved SFMS (Σ_{SFR} versus Σ_*), we also find that Σ_{H_2} traces Σ_*, which we hereafter refer to as the molecular gas main sequence (MGMS). We fit each of the above relations using the orthogonal distance regression (ODR) fitting method

[12] Adopting different S/N cuts between 1.5 and 3 does not significantly alter the slopes of the scaling relations presented here, and none of our conclusions are affected. We choose to adopt a loose cut in CO in order to maximize the number of spaxels that can be used in this work.

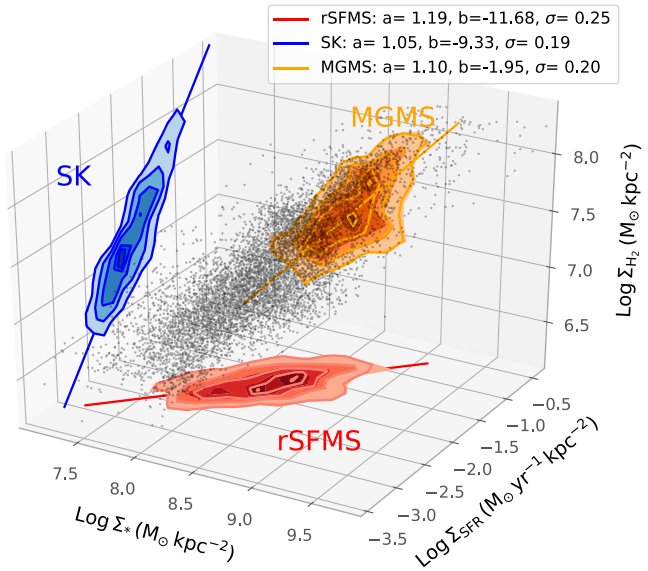

Figure 1. The 3D distribution between Σ_*, Σ_{H_2}, and Σ_{SFR}, computed for 5383 spaxels (black points) identified as star-forming regions taken from 14 MaNGA main-sequence galaxies. The contours show the results projected on the 2D planes (red: SFMS; blue: SK; orange: MGMS), with the contour levels corresponding to 20%, 40%, 60%, 80%, and 90% of the density peaks. The best-fit parameters and associated scatters (σ) based on ODR fitting are given in the legend.

Table 1
Best-fit Parameters (a and b) and Associated Scatters (σ) for the 2D Scaling Relations

Relation	a (ODR)	b (ODR)	σ (ODR)
rSFMS (Σ_{SFR}vs. Σ_*)	1.19 ± 0.01	−11.68 ± 0.11	0.25
SK (Σ_{SFR}vs. Σ_{H_2})	1.05 ± 0.01	−9.33 ± 0.06	0.19
MGMS (Σ_{H_2} vs. Σ_*)	1.10 ± 0.01	−1.95 ± 0.08	0.20

with a power law parameterized as follows:

$$\log_{10}\Sigma_{SFR} = a * \log_{10}\Sigma_* + b \quad (1)$$

$$\log_{10}\Sigma_{SFR} = a * \log_{10}\Sigma_{H2} + b \quad (2)$$

$$\log_{10}\Sigma_{H2} = a * \log_{10}\Sigma_* + b. \quad (3)$$

The best-fit parameters are shown in the legends of Figure 1 and in Table 1.

3.2. Resolved Star-forming Main Sequence

Figure 2 shows the Σ_{SFR} versus Σ_* relation for the star-forming spaxels in our sample. We first note that the slope of the resolved MS (gray points), 1.19 ± 0.01, is higher than those ($\leqslant 1$) reported in the literature (Cano-Díaz et al. 2016, 2019; Hsieh et al. 2017; Ellison et al. 2018; Medling et al. 2018; Pan et al. 2018). It is already known that the slope is sensitive to both the fitting algorithms (e.g., ODR versus ordinary least squares) and whether the non-H II regions are excluded or not. Nonetheless, our result is still slightly higher than that reported (~ 1) by Hsieh et al. (2017), who computed Σ_{SFR} and Σ_* using the same method for 536 star-forming galaxies from the MaNGA DR13 sample with the ODR fitting. To test whether this is due to the limited number of galaxies used in this analysis, we randomly select 14 galaxies from the MaNGA DR13 star-forming population to measure the slope of the rSFMS and repeat this process 1000 times. The derived

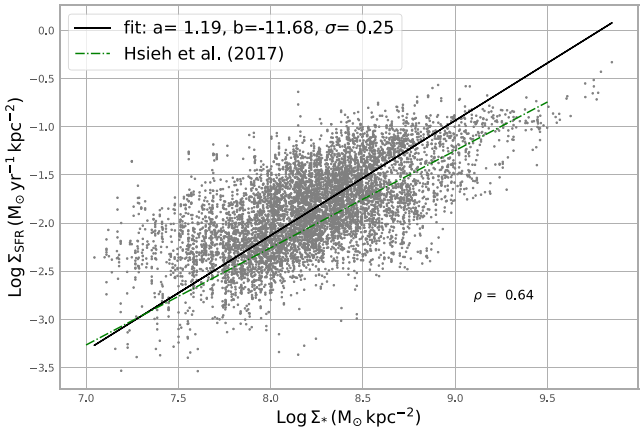

Figure 2. Spaxel-based star formation rate surface density vs. stellar mass surface density ($\Sigma_{\rm SFR}$ –Σ_*) relation (gray points) for the ALMaQUEST sample. The black solid line represents the best fit to our data. The best-fit parameters, associated scatter (σ), and the Pearson correlation coefficient (ρ) are given in the legend. The green dotted dashed line is the ODR fitting result derived by Hsieh et al. (2017) based on 536 star-forming main-sequence galaxies in the MaNGA DR13 sample.

mean slope of the 1000 trials is 1.11 $\pm$ 0.16. The slope of our CO sample is therefore consistent ($\sim$0.5σ) with the Monte Carlo result, implying that the steeper slope obtained for our sample is likely due to the small number of the CO targets instead of a biased population.

3.3. SK and Extended SK Relation

The SK relation has been measured to have a power-law index (N) ranging from 0.5 to 3 (see Bigiel et al. 2008), depending on not only the star formation rate or gas tracer (Gao & Solomon 2004; Bigiel et al. 2008) but also the physical scale used when computing the surface density (Onodera et al. 2010; Kreckel et al. 2018). On larger scales (e.g., averaged over the entire galaxy), N is superlinear ($\sim$1.4) for H_2 tracers, such as CO, and is close to unity for dense gas tracers, such as HCN or HCO+ (e.g., Gao & Solomon 2004). On the other hand, at smaller scales (kpc or sub-kpc), $N \sim 1$ or even lower for CO-based H_2 mass (Bigiel et al. 2008; Rahmani et al. 2016; Bolatto et al. 2017; Kreckel et al. 2018). In this work, our data is well fitted by a power law with exponent $N \sim 1.05 \pm 0.01$ (the left panel of Figure 3), in good agreement with recent studies on kpc/sub-kpc scales (Bigiel et al. 2008; Leroy et al. 2013; Bolatto et al. 2017; Kreckel et al. 2018; Dey et al. 2019). It is worth noting that the slope of the SK relation is not affected by the cutoff in the H_2 limit associated with the S/N cut in the CO flux. This is because the number density of spaxels in that regime is relatively sparse.

Next, we explore the so-called extended SK relation (Shi et al. 2011, 2018), in which SFR is parameterized as SFR $\propto (\Sigma_{H_2} \times \Sigma_*^{\beta})^a$. It has been suggested that the scatter of the extended SK relation can be reduced when adopting $\beta = 0.5$, which is often attributed to the effect of the midplane pressure (Ostriker et al. 2010; Shi et al. 2011; Hughes et al. 2013). To test whether the extended SK relation applies to our sample, we first color code our data with Σ_* in the left panel of Figure 3. It can be seen that there is no apparent dependence of the scatter on Σ_*, contrary to expectations from an extended SK model. On the other hand, a tendency of increasing H_2 with increasing Σ_* is revealed, which will be discussed in Section 3.4. To further explore the possibility of a Σ_* component to the SK relation, we vary the exponent β between -1 and 1 and compute the scatter of the best fit for a given β. In the inset of the right panel of Figure 3, we plot the residual scatter against the power exponent β. It is found that the scatter of the SK relation reaches a minimum value at $\beta = -0.3$ but is not significantly different from the case in the original SK relation (i.e., $\beta = 0$). The scatter even becomes larger when adopting the "canonical" value of 0.5.

The extended SK relation with the optimal power exponent ($\beta = -0.3$) is shown in the right panel of Figure 3. Overall, across the range in the stellar mass surface density of our data, we do not find a significant improvement as seen in Shi et al. (2018) when adopting the extended SK relation. However, we note that our sample spans only 1.5 orders of magnitude in Σ_* down to 10^7 $M_\odot$ kpc^{-2}, while Shi et al. (2018) covers a much wider range in Σ_* ($\sim$5 orders of magnitude).

3.4. Molecular Gas Main Sequence

Unlike the rSFMS and SK relations, the relationship between Σ_{H_2} and Σ_* has not been explored much in the literature. A positive correlation between these two quantities with a large spread was previously shown in Wong et al. (2013) and Barrera-Ballesteros et al. (2018). In fact, this trend may be expected within individual galaxies, since both the gas and stellar mass profiles generally decline with radius in spiral galaxies (e.g., Casasola et al. 2017). However, it is not clear whether there exists a universal scaling relation applicable to all systems.

In Figure 4, we explore the spaxel-based correlation between these two quantities, color-coded by sSFR. We see that Σ_{H_2} is almost linearly dependent on Σ_* with a scatter of $\sim$0.2 dex, forming the MGMS. Again the H_2 limit has little impact on the derived slope of the MGMS in our data. It is found that spaxels with higher sSFR tend to lie on the upper end of the MGMS, meaning that the star formation is boosted in regions with enhanced gas fraction, as seen in spatially unresolved data (Saintonge et al. 2017). The effect of the gas fraction on sSFR locally will be further discussed in a companion ALMaQUEST paper (Ellison et al. 2019).

4. Discussion

In this work, we have established a three-way scaling relationship between $\Sigma_{\rm SFR}$, Σ_*, and Σ_{H_2} on kpc scales. Each pair of these three parameters exhibits a tight correlation with a scatter of $\sim$0.19–0.25 dex. Among the three relations, two already well known: SK relation ($\Sigma_{\rm SFR}$ versus Σ_{H_2}) and the rSFMS ($\Sigma_{\rm SFR}$ versus Σ_*), while the third one, the MGMS between Σ_{H_2} and Σ_*, is shown convincingly here for the first time. It is natural to ask: which of these correlations are more fundamental?

To quantify the relative importance among the three 2D relations, we compute Pearson correlation coefficients (ρ) for each of them (shown in Figures 2–4). This analysis shows that the SK relation has the strongest correlation, followed by the MGMS and then the rSFMS. Indeed, the SK relation is physically the most intuitive as stars form directly from the molecular clouds. It also has the smallest scatter of the three. On the other hand, the physical reason behind the MGMS is less obvious. We consider two possible explanations for the presence of this correlation. In the first scenario, the contribution of dark matter to the gravitational potential of

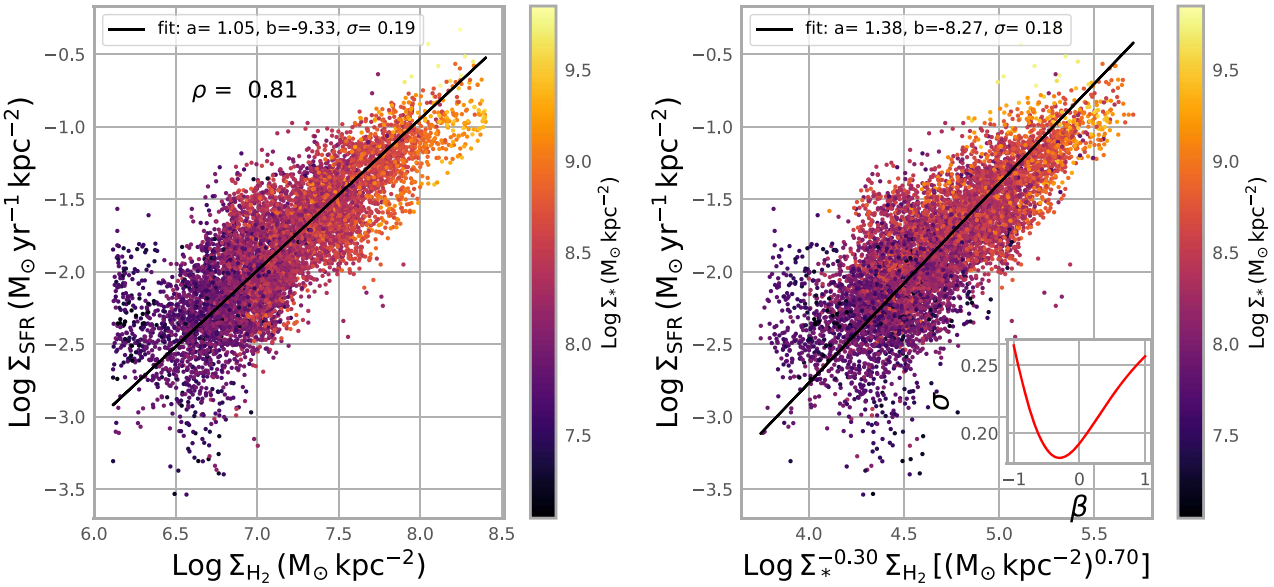

Figure 3. Spaxel-based Schmidt–Kennicutt (left panel) and extended Schmidt–Kennicutt (right panel) relations in our sample. The black solid lines show the best fits to our data. The best-fit parameters, associated scatters (σ), and the Pearson correlation coefficient (ρ) are given in the legend. The inset of the right panel shows the associated scatter of the extended SK relation as a function of the power exponent β.

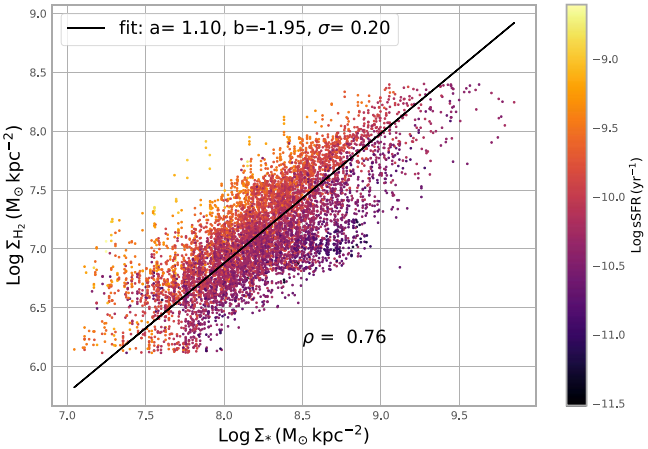

Figure 4. Spaxel-based molecular gas main-sequence (Σ_{H_2}–Σ_*) relation, color-coded by sSFR. The black solid line shows the best fit to our data. The best-fit parameters, associated scatter (σ), and the Pearson correlation coefficient (ρ) are given in the legend.

the disk is negligible compared to baryonic components. Therefore, the local potential well of the disk is primarily set by the local Σ_* given that the surface molecular gas fraction $f_{\rm gas}$ (defined as $\Sigma_{H_2}/(\Sigma_{H_2}+\Sigma_*)$) in our sample is on the order of 10% only. As a consequence, the gas follows the distribution of stellar mass, leading to the $\Sigma_{H_2}-\Sigma_*$ linear correlation. In this scenario, the correlation between Σ_{H_2} and Σ_* might be expected to break down at higher redshifts where gas masses can exceed stellar masses (Isbell et al. 2018; Tacconi et al. 2018). Alternatively, if the dark matter dominates the mass distributions, both stars and gas will respond to the same gravity. In this case, the correlation between Σ_{H_2} and Σ_* is caused by the underlying gravitational potential. Therefore, the $\Sigma_{H_2}-\Sigma_*$ relation will still hold regardless of gas fraction. Dynamical measurements and the studies of the $\Sigma_{H_2}-\Sigma_*$ relation as a function of cosmic time will shed light on the origin of the gas and stellar mass correlation.

Having established the MGMS, here we provide a plausible explanation to the empirical rSFMS. If $\Sigma_{\rm SFR}\propto{\Sigma_{H_2}}^a$ and $\Sigma_{H_2}\propto\Sigma_*^b$, one would expect $\Sigma_{\rm SFR}\propto\Sigma_*^{a*b}=\Sigma_*^{\rm it\ c}$. In our case, c is measured to be 1.19, close to 1.16, the product of a (1.05) and b (1.10). Among the three relations, the rSFMS has the largest scatter ($\sigma=0.25$) and is close to the square root of the quadratic sum of the scatters ($\sigma=0.28$) from the SK (0.19) and MGMS (0.20) relations. Furthermore, the rSFR also has the smallest Pearson correlation coefficient. All this suggests that rSFMS could be a natural consequence of the other two relations. Finally, we note that our analyses presented are restricted to the star-forming spaxels of MS galaxies. The scaling relations of the retired spaxels and for galaxies deviated from the MS will be further explored in future works (L. Lin et al. 2019, in preparation).

5. Summary

Combining the ALMA ^{12}CO(1 − 0) and MaNGA observations of 14 MS galaxies taken from the ALMaQUEST survey, we investigate the relationships between the surface densities of star formation rate, molecular gas, and stellar mass in star-forming spaxels, aiming at understanding the origin of the rSFMS. Our results can be summarized as follows.

1. The three quantities, $\Sigma_{\rm SFR}$, Σ_{H_2}, and Σ_*, computed at kpc scales, form a 3D linear (in log) relation with dispersion.
2. The 2D projections in each pair of these three parameters show tight correlations: $\Sigma_{\rm SFR}\propto\Sigma_*^{1.19}$ (the rSFMS), $\Sigma_{\rm SFR}\propto{\Sigma_{H_2}}^{1.05}$ (the SK relation), and $\Sigma_{H_2}\propto\Sigma_*^{1.10}$ (MGMS).
3. The power-law exponent (1.05) of the SK relation in our sample is in good agreement with other recent studies at kpc scales. We also investigate the extended SK law in which a Σ_* dependence is introduced, and we find no significant improvement in the scatter of the relation.
4. The existence of an MGMS implies that either stellar mass dominates the local gravitational potential of the disks or both stars and gas follow the same spatial

distributions in response to the gravity set by the underlying total mass.

5. The scatter and correlation analyses suggest that the rSFMS can be naturally explained by the combination of the SK and MGMS relations.

We thank the anonymous referee for helpful comments that improved the clarity of this work. This work is supported by the Academia Sinica under the Career Development Award CDA-107-M03 and the Ministry of Science & Technology of Taiwan under the grants MOST 107-2119-M-001-024- and MOST 108-2628-M-001-001-MY3. R.M. acknowledges ERC Advanced Grant 695671 "QUENCH." We thank M. Hani for providing helpful comments to this work. L.L. and H.-A.P. thank U. of Victoria for hosting during the visit to work on this project.

This paper makes use of the following ALMA data: ADS/JAO.ALMA#2015.1.01225.S, ADS/JAO.ALMA#2017.1.01093.S, ADS/JAO.ALMA#2018.1.00558.S, ADS/JAO.ALMA#2018.1.00541.S. ALMA is a partnership of ESO (representing its member states), NSF (USA) and NINS (Japan), together with NRC (Canada), MOST and ASIAA (Taiwan), and KASI (Republic of Korea), in cooperation with the Republic of Chile. The Joint ALMA Observatory is operated by ESO, AUI/NRAO and NAOJ.

SDSS-IV is managed by the Astrophysical Research Consortium for the Participating Institutions of the SDSS Collaboration including the Brazilian Participation Group, the Carnegie Institution for Science, Carnegie Mellon University, the Chilean Participation Group, the French Participation Group, Harvard–Smithsonian Center for Astrophysics, Instituto de Astrofísica de Canarias, The Johns Hopkins University, Kavli Institute for the Physics and Mathematics of the universe (IPMU)/University of Tokyo, Lawrence Berkeley National Laboratory, Leibniz Institut für Astrophysik Potsdam (AIP), Max-Planck-Institut für Astronomie (MPIA Heidelberg), Max-Planck-Institut für Astrophysik (MPA Garching), Max-Planck-Institut für Extraterrestrische Physik (MPE), National Astronomical Observatory of China, New Mexico State University, New York University, University of Notre Dame, Observatário Nacional/MCTI, The Ohio State University, Pennsylvania State University, Shanghai Astronomical Observatory, United Kingdom Participation Group, Universidad Nacional Autónoma de México, University of Arizona, University of Colorado Boulder, University of Oxford, University of Portsmouth, University of Utah, University of Virginia, University of Washington, University of Wisconsin, Vanderbilt University, and Yale University.

ORCID iDs

Lihwai Lin https://orcid.org/0000-0001-7218-7407
Hsi-An Pan https://orcid.org/0000-0002-1370-6964
Sara L. Ellison https://orcid.org/0000-0002-1768-1899
Francesco Belfiore https://orcid.org/0000-0002-2545-5752
Yong Shi https://orcid.org/0000-0002-8614-6275
Sebastián F. Sánchez https://orcid.org/0000-0001-6444-9307
Bau-Ching Hsieh https://orcid.org/0000-0001-5615-4904
Kate Rowlands https://orcid.org/0000-0001-7883-8434

References

Barrera-Ballesteros, J. K., Heckman, T., Sánchez, S. F., et al. 2018, ApJ, 852, 74
Bigiel, F., Leroy, A., Walter, F., et al. 2008, AJ, 136, 2846
Bolatto, A. D., Wolfire, M., & Leroy, A. K. 2013, ARA&A, 51, 207
Bolatto, A. D., Wong, T., Utomo, D., et al. 2017, ApJ, 846, 159
Brinchmann, J., Charlot, S., White, S. D. M., et al. 2004, MNRAS, 351, 1151
Bundy, K., Bershady, M. A., Law, D. R., et al. 2015, ApJ, 798, 7
Cano-Díaz, M., Ávila-Reese, V., Sánchez, S. F., et al. 2019, MNRAS, 488, 3929
Cano-Díaz, M., Sánchez, S. F., Zibetti, S., et al. 2016, ApJL, 821, L26
Casasola, V., Cassarà, L. P., Bianchi, S., et al. 2017, A&A, 605, A18
Cooper, M. C., Newman, J. A., Coil, A. L., et al. 2007, MNRAS, 376, 1445
Daddi, E., Dickinson, M., Morrison, G., et al. 2007, ApJ, 670, 156
Dey, B., Rosolowsky, E., Cao, Y., et al. 2019, MNRAS, 488, 1926
Dressler, A. 1980, ApJ, 236, 351
Elbaz, D., Daddi, E., Le Borgne, D., et al. 2007, A&A, 468, 33
Ellison, S. L., Sánchez, S. F., Ibarra-Medel, H., et al. 2018, MNRAS, 474, 2039
Ellison, S. L., Thorp, D. M., Lin, L., et al. 2019, MNRAS, submitted
Fischera, J., & Dopita, M. 2005, ApJ, 619, 340
Gao, Y., & Solomon, P. M. 2004, ApJ, 606, 271
Hsieh, B. C., Lin, L., Lin, J. H., et al. 2017, ApJL, 851, L24
Hughes, A., Meidt, S. E., Colombo, D., et al. 2013, ApJ, 779, 46
Isbell, J. W., Xue, R., & Fu, H. 2018, ApJL, 869, L37
Kauffmann, G., Heckman, T. M., Tremonti, C., et al. 2003, MNRAS, 346, 1055
Kauffmann, G., White, S. D. M., Heckman, T. M., et al. 2004, MNRAS, 353, 713
Kennicutt, R. C., Jr. 1998, ApJ, 498, 541
Kreckel, K., Faesi, C., Kruijssen, J. M. D., et al. 2018, ApJL, 863, L21
Krumholz, M. R., & McKee, C. F. 2005, ApJ, 630, 250
Leroy, A. K., Walter, F., Sandstrom, K., et al. 2013, AJ, 146, 19
Lin, L., Belfiore, F., Pan, H.-A., et al. 2017, ApJ, 851, 18
Lin, L., Dickinson, M., Jian, H.-Y., et al. 2012, ApJ, 756, 71
Lin, L., Jian, H.-Y., Foucaud, S., et al. 2014, ApJ, 782, 33
Medling, A. M., Cortese, L., Croom, S. M., et al. 2018, MNRAS, 475, 5194
Murray, N. 2011, ApJ, 729, 133
Noeske, K. G., Faber, S. M., Weiner, B. J., et al. 2007, ApJL, 660, L47
Onodera, S., Kuno, N., Tosaki, T., et al. 2010, ApJL, 722, L127
Ostriker, E. C., McKee, C. F., & Leroy, A. K. 2010, ApJ, 721, 975
Pan, H.-A., Lin, L., Hsieh, B.-C., et al. 2018, ApJ, 854, 159
Rahmani, S., Lianou, S., & Barmby, P. 2016, MNRAS, 456, 4128
Saintonge, A., Catinella, B., Tacconi, L. J., et al. 2017, ApJS, 233, 22
Sánchez, S. F., Pérez, E., Sánchez-Blázquez, P., et al. 2016, RMxAA, 52, 21
Sánchez, S. F., Rosales-Ortega, F. F., Jungwiert, B., et al. 2013, A&A, 554, A58
Schmidt, M. 1959, ApJ, 129, 243
Shi, Y., Helou, G., Yan, L., et al. 2011, ApJ, 733, 87
Shi, Y., Yan, L., Armus, L., et al. 2018, ApJ, 853, 149
Speagle, J. S., Steinhardt, C. L., Capak, P. L., & Silverman, J. D. 2014, ApJS, 214, 15
Tacconi, L. J., Genzel, R., Saintonge, A., et al. 2018, ApJ, 853, 179
Vogt, F. P. A., Dopita, M. A., & Kewley, L. J. 2013, ApJ, 768, 151
Vulcani, B., Poggianti, B. M., Moretti, A., et al. 2019, MNRAS, 488, 1597
Whitaker, K. E., van Dokkum, P. G., Brammer, G., et al. 2012, ApJL, 754, L29
Wong, T., Xue, R., Bolatto, A. D., et al. 2013, ApJL, 777, L4
Wuyts, S., Förster Schreiber, N. M., Nelson, E. J., et al. 2013, ApJ, 779, 135